IEEE Photonics Journal
An IEEE Photonics Society Publication

Open Access

Rare Earth-Doped Microfiber Bragg Grating Refractive Index Sensor With Self-Photothermal Manipulation

Volume 13, Number 3, June 2021

Yongkang Zhang
Yi Yin
Jiexuan Cai
Xueting Long
Zhiyuan Xu
Yang Ran
Bai-Ou Guan

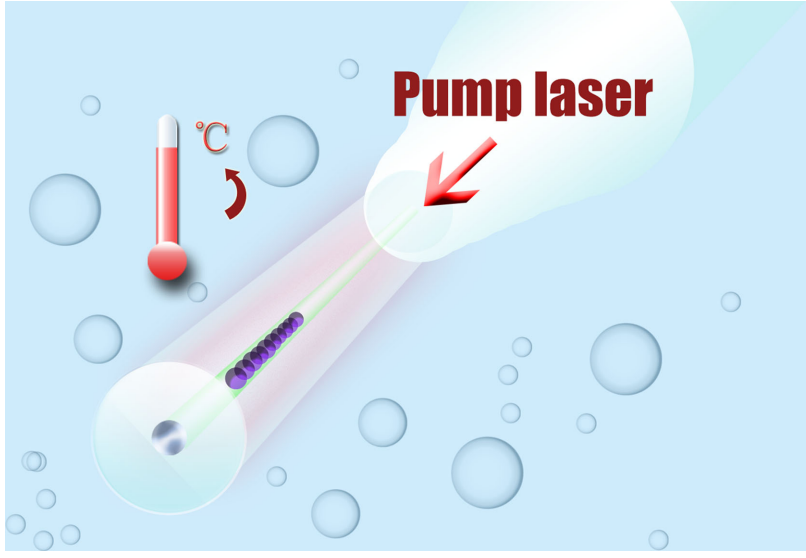

DOI: 10.1109/JPHOT.2021.3081675

IEEE photonics SOCIETY
IEEE

Rare Earth-Doped Microfiber Bragg Grating Refractive Index Sensor With Self-Photothermal Manipulation

Yongkang Zhang, Yi Yin, Jiexuan Cai, Xueting Long, Zhiyuan Xu, Yang Ran, and Bai-Ou Guan

Guangdong Provincial Key Laboratory of Optical Fiber Sensing and Communications, Institute of Photonics Technology, Jinan University, Guangzhou 510632, China

DOI:10.1109/JPHOT.2021.3081675

Manuscript received April 19, 2021; revised May 11, 2021; accepted May 14, 2021. Date of publication May 18, 2021; date of current version June 4, 2021. This work was supported in part by the National Natural Science Foundation of China (NSFC) under Grants 61775082, U1701268, in part by the Science and Technology Program of Guangzhou under Grant 202102010113, and in part by the Fundamental Research Funds for the Central Universities. Corresponding author: Yang Ran (e-mail: tranyang@jnu.edu.cn).

Abstract: We demonstrate a microfiber Bragg grating as the reflective refractometer with the function of self-photoheating. The rare earth-doped fiber provides not only the photosensitivity to the UV modulation but also the effective pump laser absorption and photoheating conversion. The rare earth-doped microfiber Bragg grating, which is cladding-removed by the hydrofluoric acid, can detect the tiny refractive index change with a resolution of 10^{-4} RIU scale. The self-photoheating could be realized by 980 nm pump absorption and non-radiative transition process of the ytterbium and erbium ions, which are well-preserved by the core structure after etching. Monitored by the reflective grating signal, the photoheating can manipulate 30 °C increase of the device in the air, 8 °C in the ethanol, and 4 °C in the water. The second time-scale heating/cooling response allows the sensor to act as ad optical switch for engineering temperature. The work may open a new route for accelerative biosensing and pollutant determination and treatment.

Index Terms: Microfiber, fiber Bragg grating, refractive index sensing, rare earth-doped fiber, laser pump, self-photothermal.

1. Introduction

Optical fiber sensors for the determination of ambient refractive index (RI) have attracted increasing attention due to their capability in mediating bio-chemo molecular reactions [1]–[3]. With the significantly strengthened evanescent field, microfiber further enables the interplay between the propagating light and surrounding medium and presents the higher interfacial RI sensitivity [4]. Moreover, the microfiber structure is intrinsically compatible with the communication fiber system, bridging the gap between fields of fiber optics and micro/nano-photonics [5]–[8]. Bragg grating in the microfiber (μFBG) adds features of reflective signal operation, compactness, narrow bandwidth signal, and wavelength multiplexing, facilitating the fabrication of miniature fiber detectors and establishment of bio/chemical sensing network [9], [10]. The μFBGs aiming at the detection of gas [11], acidity [12], nucleic acid [13]–[15], and protein/antigen [16]–[20] were reported, showing a promising development. However, passively sensing the bio/chemical reagents is not enough for all of the circumstances. For example, the antibody-antigen binding efficiency could be enhanced in a

moderately thermal environment. Some samples containing hazardous substances require heating treatment after detection to reduce the toxic risk. Therefore, the integration of the photothermal functionality using μFBG is highly pursued and requires further investigation.

Several photo-thermal transition materials were utilized to realize the photoheating functionality of the fiber sensor through surface modification. 2D materials like graphene [21], [22], black phosphorus, and graphene hybrid nanocomposites [23], [24] were exploited to generate heat by drawing the light energy via the evanescent field of the microfiber to realize the applications of phase shift and switch, optical biostability and photothermal induced cell necrosis. High absorption coatings, such as black ink [25] and pure amorphous carbon [26] were also utilized to achieve DNA melt analysis and amplification as well as hyperthermia-induced cell death. The colloidal gold nanoparticle solution was another attempt to enable the phase shift and switch mediated by the localized surface plasmonic effect [27].

In contrast to the outer functionalization on the fiber, the intracore dopants activated photothermal is an appealing alternative because it can overcome the limitations, such as the laborious and time-consuming decoration of the materials, risk of coating fall-off, low pump utilization, and difficulty increasing in the bio/chemoreceptor immobilization. Furthermore, aggregation and oxidization could also be avoided as a result of the enclosed dopants in the silica core. Erbium-ytterbium (Er/Yb) co-doped optical fiber allows the effective pump absorption derived from the high-density clusters of ytterbium ions and a large portion of the non-radiative transition that originates from the erbium ions, providing excellent opportunity in developing the intracore self-heated fiber Bragg grating device [28]. For achieving the RI sensing, thinned Er/Yb co-doped fiber is required. Nevertheless, the flame taper method, that is, the current workhorse for the fabrication of microfiber, is inadequate because minimizing fiber core may lead to the dissipation of the active dopants, which would reduce the pump adsorption and rate of photo-thermal conversion [29], [30].

In this paper, we harness the etched Er/Yb co-doped active fiber Bragg grating as the tip refractometer with self-photoheating functionality. The photosensitivity of the fiber guarantees the strong grating formation for generating the narrow bandwidth signal, which is required by the high-resolution interrogation. The cladding etching using hydrofluoric acid not only maintains the integrity of the rare earth doped core structure but also allows the guiding mode to penetrate into the ambient medium for peeping the RI alteration [31]. The μFBG can capture a tiny RI change as low as 4×10^{-4} RIU. The self-photoheating could be implemented by injecting the pump photons, and the temperature elevation could be measured by the grating. Under 500 mW pumping, the μFBG could be heated by an amount of 30 °C in the air, 8 °C in the ethanol, and 4 °C in the water. The pump switch test shows that the heater could respond to the on and off instantaneously, enabling the dynamic self-heat governing capability, which may motivate the accelerative biosensing and volatile chemical solution treatment.

2. Experimental Setup

The optical fibers used in this study are the Erbium-Ytterbium co-doped active fiber (7/125 μm, Coractive Inc., Canada) and standard single-mode fiber (SMF-28, 8/125μm, Corning, Ltd., USA). The pure 100%-ethanol was acquired from HUSHI (China). 40% Hydrofluoric acid (HF) was purchased from MaCKLIN (AR,40%). All the chemicals were of analytical grade. Deionized (DI) water was used throughout the experiment. The 193 nm Excimer laser (Compex 110, Coherent co, Ltd, USA) was used to conduct the refractive index change on the microfiber. A broad-band light source (BBS, GoLigtht Ltd., China) was utilized to launch a continuous spectrum light ranging from 1520 to 1580 nm as a background reference. A 980 nm Pump Light Source (Golight, China) was used to provide light energy for the photothermic manipulation. A high-resolution optical spectrum analyzer (OSA, BOSA-light, Argon Photonics, Ltd, Spain) with a spectral resolution of 0.1 pm was employed to log the tiny spectral variation of the output spectrum. A hand-held refractometer (PAL-RI, ATAGO, Japan) was used to calibrate the refractive index of the solution. The Hotplate & Magnetic Stirrer was obtained from DLAB (MS-H-ProT, DLAB Scientific Co., Ltd, China). A tube

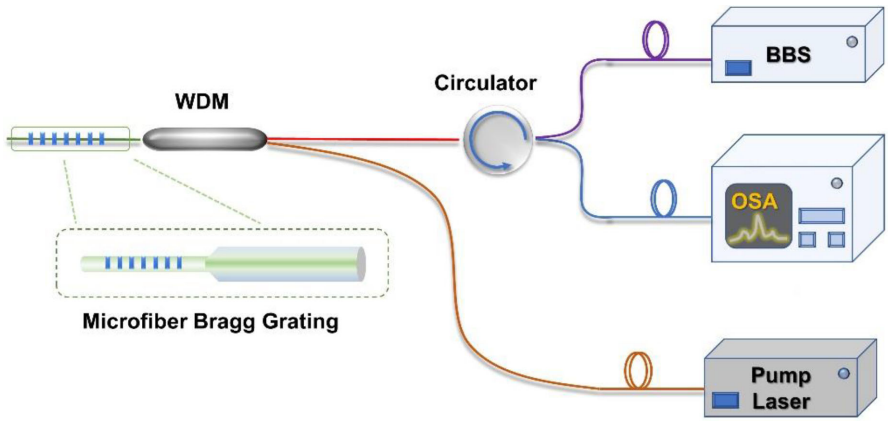

Fig. 1. Schematic of the optical setup for Er/Yb co-doped μFBG device. WDM: wavelength division multiplexer; BBS: broad-band source; OSA: optical spectral analyzer.

oven was purchased from ECOM (ECOM column oven LCO 102, Czech). An optical microscope was used to characterize the diameter of the optical fiber.

Fig. 1. schematically depicts the experimental setup. The BBS and OSA were linked into the system for monitoring the reflection spectrum of the μFBG via an optical circulator. A pumping light source with a central wavelength of 980 nm served as the photon injector via a wavelength division multiplexer (WDM,1550/980). The pump laser traveled to the μFBG which was written in the Er/Yb co-doped core for actuating the photo-thermal conversion.

3. Fabrication of Rare-earth Doped Microfiber Bragg Grating

The inscription method incorporating a 193 nm excimer laser (Compex 110, Coherent, Inc.,) and the phase masks was adopted to imprint the Bragg modulation in the rare earth-doped fiber. The laser beam profile is a rectangle shape with the size of 4 mm $\times$ 20 mm (W $\times$ H). In this research, the pulse energy was set to 115 mJ, and thus an energy density of 250 mJ/cm^2 was obtained through a cylindrical lens that converges the beam in the H dimension. The repetition rate of the laser emission was set to 20 Hz. The phase mask with a pitch of 1075.5 nm was utilized to guarantee the Bragg resonance within the operation range of the BOSA (1520 nm–1570 nm).

The FBG inscription included a two-step process for fabricating the phase-shifted Bragg grating in the active fiber [17], [32]. First, half of Bragg grating was obtained through a 1-minute exposure. Second, the phase mask was precisely displaced with half of the pitch ($\sim$538 nm) through a high-precision linear translational stage for introducing a phase shift into the refractive index modulation on the fiber core. The laser was moved by a distance across an entire beam width of 4 mm then irradiated on a blank part of the fiber that was closed to the already-made half-Bragg grating for 1 minute. The total length of the grating was 8 mm. Fig. 2 (a) portrayed the transmission spectrum of the FBG with a total reflectivity of 99.5%. A notch signal locating at $\sim$1556 nm could be clearly observed within the stopband, indicating that a phase shift was successfully introduced into the modulation structure. The phase-shifted signal with finer linewidth guarantees the implementation of high-resolution interrogation for obtaining a lower RI detection limit [17].

For enabling the ambient refractive index sensing capability, cladding removal was needed for the active fiber Bragg grating to facilitate the guiding light interplaying with the ambient solution through the evanescent field. The goal could be achieved by immersing the FBG tip in 40% HF solution for 50 min, 20% HF solution for 15 min, and 10% HF solution for 7 min in sequence. The time control of the last etching phase enabled the precise engineering of the fiber diameter. The spectral reflection evolution from the FBG to μFBG was monitored throughout the etching process

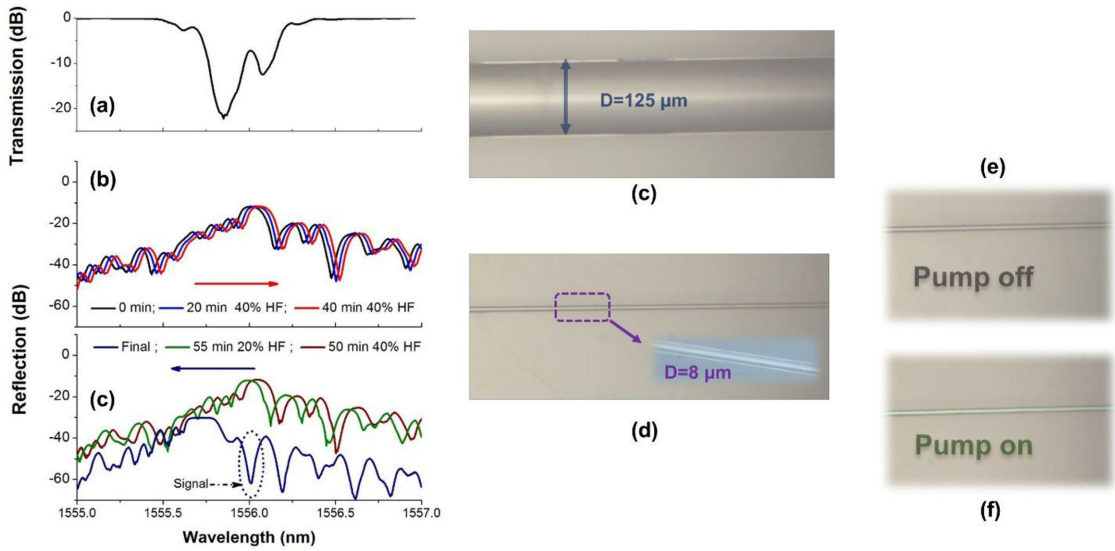

Fig. 2. (a) Transmission spectrum of the FBG. Reflection spectral variation in (b) the first phase etching (spectral red-shift), and (c) the second phase etching (spectral blue-shift). The contrast of the microscopic images between (d) the pre-etched fiber and (e) etched fiber; inset: the zoom-in etched fiber. The microscopic images of the microfiber with pump laser (e) off and (f) on. HF: Hydrofluoric acid; D: diameter of the fiber.

for the auxiliary verification of the final diameter. The diameter error could be controlled to as low as 0.2 μm. Fig. 2(b) recorded the first stage of the rough etching from start to 40 min 40% HF bathing. The side-lobes were seen in the reflection due to the lack of apodization in the inscription; they, nevertheless, would not affect the effective signal in the measurement. The wavelength notch signal exhibited a positive response from 1556.14 nm to 1556.19 nm. The chemical reaction between the HF acid and the silica glass surface thermalized the solution that gave rise to the redshift of the notch signal [33]. The second stage that included the rest part of the process was then logged in Fig. 2(c). In contrast to the first stage, the notch signal moved reversely and presented a blueshift tendency. At the end of the precise etching using 10% HF solution, a total blueshift of 0.14 nm can be observed because the cladding of the FBG was substantially removed, and the expansion of the evanescent field resulted in the decrease of the effective refractive index of the fiber. The Bragg reflection countered a 20 dB attenuation, although, the effective Bragg signal could still survive in the different ambientes, such as the ethanol and water, in the following experiment. Fig. 2(c) and (d) make a comparison between the normal fiber and the etched fiber. According to Fig. 2(d), the diameter of μFBG was measured to about 8 μm. Unlike the μFBG originating from the flame tapering [29], the miniaturization of μFBG was realized by HF etching, which could facilitate the maintaining of the core structure. We delivered the 980- pump laser to the μFBG region. Compared with the pump-off state (Fig. 2(e)), the pump activation drove the μFBG to emit the green fluorescence (Fig. 2(f)), which was mainly derived from the upconversion of the Erbium ions that absorbed the pump laser. The bright green fluorescence emitted from the thinned fiber shed light on the preservation of the density of the rare-earth dopants in the core after tapering. The final reflection spectrum of the grating with a high SNR Bragg signal also confirms well with the conservation of the core structure of the μFBG.

4. Sensing Characterization of RD-μ-FBG

Thinned fiber enables the ambient RI response mediated by the enlargement of the evanescent field. We had surveyed the RI sensitivity of the RD-μFBG in the first place. A series of liquid

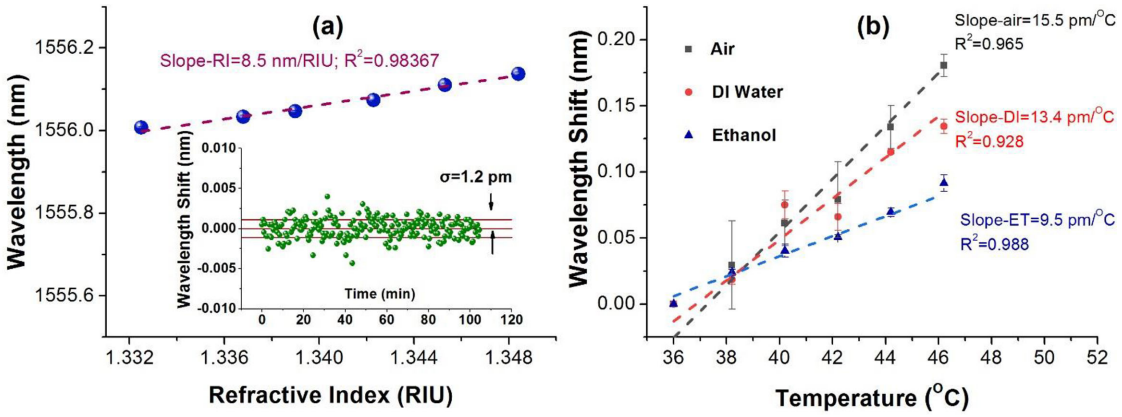

Fig. 3. Response curve of the μFBG regarding ambient RI. Inset: long-term wavelength stability of μFBG in the room temperature DI water. Temperature response of μFBG in different ambients. Error bars indicate the standard deviations of three independent measurements, and below are the same.

samples with different RI ranging from 1.33 to 1.348 were prepared by mixing the ethanol and deionized water with different volume ratios. Fig. 3(a) showed the wavelength response of the RD-μFBG with respect to the liquid samples. It should be notified that each point was plotted by three independent measurements. The negligible error bars proved the fidelity of the RI sensing using the proposed RD-μFBG. By fitting the measured points with a linear curve, we quantified the RI sensitivity (S_{RI}) of the RD-μFBG to about 8.5 nm/RIU ($R^2 = 0.98367$). Although the RI sensitivity presented in this work is not as high as the long-period grating and the modal interferometer, which present the RI sensitivity ranging from several hundred and even tens of thousands nm per RI unit, good stability and narrow linewidth of the μFBG can offer the RI sensitivity improvement by the high-resolution interrogation. The long-term stability test shown in the inset of Fig. 3(a) was utilized to showcase the limit resolution of the sensor. By bathing the RD-μFBG into pure ethanol for 120 min, the wavelength jittering of the notch was interrogated. The standard deviation (σ) of wavelength drift was estimated to about 1.2 pm. Therefore, according to the limit resolution described by Eq. (1)

$$\text{Resolution limit} = \frac{3\sigma}{\text{Sensitivity}} \tag{1}$$

the proposed sensor possessed a limit resolution to as low as 4.24×10^{-4} RIU, manifesting the capability in transducing a tiny alteration of ambient RI to a distinguishable signal change.

To reveal the temperature responsivity, we tested the sensor in different media that were thermally operated from 36 °C to 46 °C. The results are shown in Fig. 3(b). The temperature responsivity in the air condition was about 15.5 pm/ °C ($R^2 = 0.965$), which was a little higher than conventional FBG. It could be explained by the larger influence exerted by the rare-earth dopants in the microfiber. In addition, the instability of the thermal operation from the temperature control box could also contribute to the larger error bars compared to the considerably small temperature range that corresponds to the photothermal effect. It is anticipated to be reduced by carrying out further repeated experiments and setting a larger range of temperatures. The RD-μFBG was then tested in the deionized water and pure ethanol conditions. The liquid beaker was warmed by the heating plate. We quantified the temperature sensitivity in DI water and pure ethanol to 13.4 pm/ °C ($R^2 = 0.928$) and 9.5 pm/ °C ($R^2 = 0.988$), respectively, which were both lower than the air test result. Here, apart from sensing the temperature variation in the liquid, the RD-μFBG could also detect the tiny refractive index change of the heated liquid. As the liquid temperature was elevated, the refractive index would decrease. It could be described by the thermo-optical coefficients, which could derive the modified function of wavelength shift with regard to the temperature rising

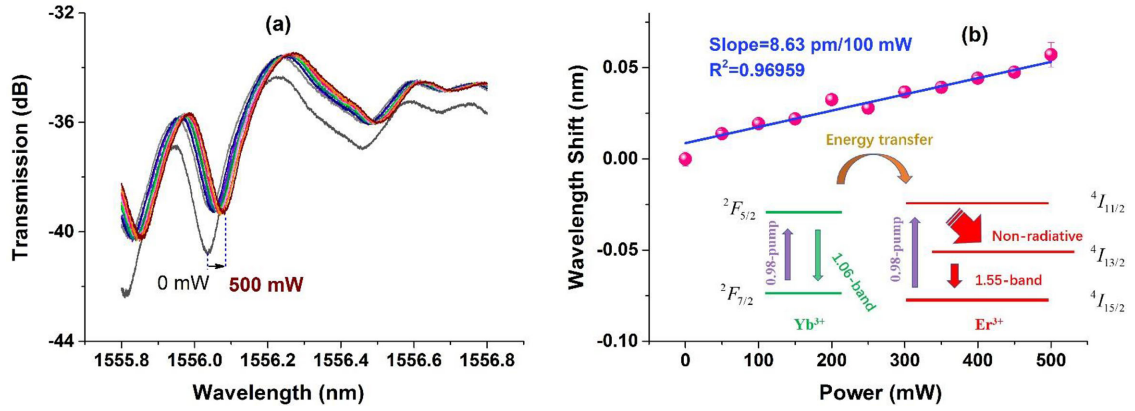

Fig. 4. (a)The spectral variation of the μFBG with the increase of the pump power from 0 mW to 500 mW in the DI water. (b) Relationship between the pump power and photoheating induced wavelength shift. Inset: simplified energy-level diagram of the Er/Yb co-doped system.

as Eq. (2)

$$\Delta\lambda = \Delta\lambda_t + \eta_{liq} \times \Delta T \times S_{RI} \tag{2}$$

$\Delta\lambda_t$ is the absolute temperature response, and η_{liq} is the thermo-optical coefficient of the liquid. The thermo-optical coefficients of pure ethanol (η_{ET}) and DI water (η_{DI}) are -3.117 $\times$ 10^{-4}/°C and -1.128$\times 10^{-4}$/ °C, respectively. Therefore, the absolute temperature sensitivity of μFBG in pure ethanol and DI water could be corrected to 12.2 pm/ °C and 14.3 pm/ °C. Regarding the regression factors in different curves, we can infer that the absolute temperature sensitivity of RD-μFBG acquired in pure ethanol is more accurate. Nevertheless, the temperature test results that involve the response to the thermal-induced RI change allow the direct interpretation of the sensor self-photoheating test results in the next step experiment.

5. Self-Photoheating of RD-μFBG

To investigate the self-photothermal effect of the sensor, we used another similarly fabricated RD-μFBG to characterize the response to the 980 nm laser pumping in the DI water. By tuning the pump laser power from 0 mW to 500 mW with an increment of 50 mW, the spectral evolution was portrayed in Fig. 4(a). It could be observed that the notch dip moved to the longer wavelength with an increase of the pump power, revealing the gradually thermal activation induced by the photon injection. As the pump power was lifted from 0 mW to 500 mW, the phase shift dip exhibited a total wavelength shift of $\sim$0.057 nm, indicating that the photo-thermal conversion acted on the μFBG. It worth noting that the overall signal elevated about 1.4 dB. It could be attributed to the amplification conducted by the erbium ions. According to Fig. 4(b), by linearly fitting the wavelength shift corresponding to the increase of the pump power, the slope was about 8.6 pm/100 mW, denoting the photo-thermal efficiency of 0.64 °C/100 mW with regard to the temperature sensitivity of RD-μFBG in DI water.

The inset of Fig. 4(b) illustrates the diagram of the energy transfer from the lanthanide dopants. Yb^{3+} and Er^{3+} embedded in the fiber core both absorb the 980 nm photons to conduct population inversion in which the electrons are pumped and transit from $^2F_{7/2}$ and $^4I_{15/2}$ levels to $^2F_{5/2}$ and $^4I_{11/2}$ level, respectively. In this type of active fiber, an overwhelmingly higher concentration of Yb^{3+} was doped to encompass Er^{3+} (Yb^{3+}/Er^{3+} = 40:1) for eliminating the quenching. A portion of excited Yb^{3+} transfers energy from $^2F_{5/2}$ to the center Er^{3+} in the $^4I_{15/2}$ level as the donor, giving rise to the excitation to $^4I_{11/2}$ level as well. The doping recipe of the fiber guarantees the effective 980 nm-pump absorption to about 500 dB per meter. The excited Er^{3+} downwardly transits to the

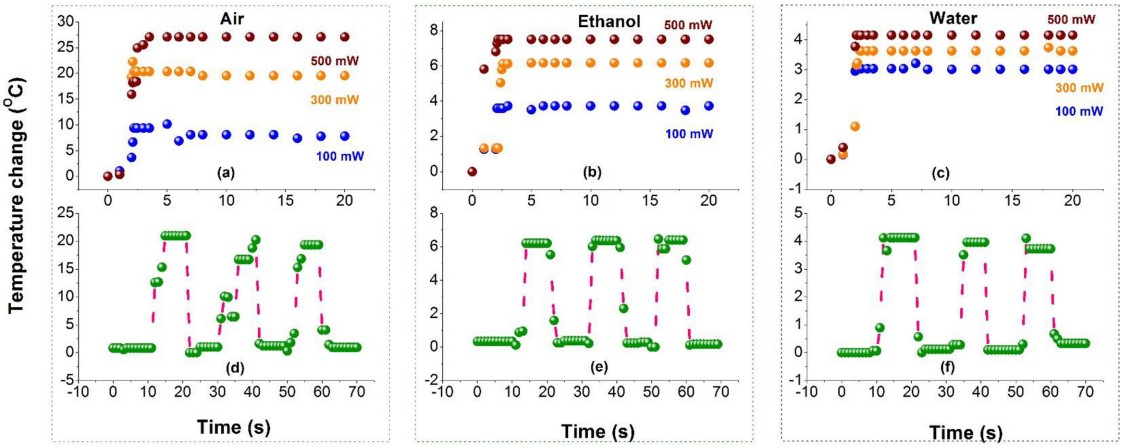

Fig. 5. The dynamic heating response of the μFBG with continuous pump with different powers in (a) the air (b) the ethanol (c) the DI water. The pump switch test using 300 mW pump power in (d) the air, (e) the ethanol, and (f) the DI water.

metastable level $^4I_{13/2}$. This non-radiative process mainly contributes to the thermal release during the pumping.

In the following, the RD-μFBG operated in air, pure ethanol, and DI water was studied to explore the photo-thermal efficacy of the sensor in different environments. The pump power was set to three typical values of 100 mW, 300 mW, and 500 mW. The spectrum was monitored in real-time. Fig. 5(a) showed the wavelength variation of RD-μFBG in the air corresponding to the pump power in which the wavelength shift could represent the temperature elevation. As the pump was added, the rare-earth ions absorbed the pump and released heat mediated by the non-radiative transition until the stable state of temperature was formed. According to the pumping gram, the temperature went to the steps regarding the pump power instantaneously (shorter than 2 seconds). The 100 mW and 300 mW pump powers would result in the temperature rising of 7 °C and 20 °C, respectively. A near 30 °C elevation could be reached by pumping the 500-mW laser.

Similar dynamic curves could also be found in the tests of pure ethanol (Fig. 5(b)) and DI water (Fig. 5(c)) but with different temperature elevation amplitudes. The ethanol could be warmed up about 8 °C in 500 mW. A 4 °C temperature rising was obtained for the DI water. The dissimilarity of the heating performance was derived from the different heat transfer rates of the environments. The heat transfer rate of water is 0.5 to 0.7 $W*m^{-1}*K^{-1}$, which is significantly larger than pure ethanol 0.18 $W*m^{-1}*k^{-1}$ and air 0.01-0.04 $W*m^{-1}*K^{-1}$.As the μFBG was self-heated, the ambient liquid would draw the heat outside the fiber and gave rise to cooling of the fiber core.

To further investigate the response of RD-μFBG in the time domain, the fast pump switch test was performed by monitoring the notch wavelength alteration during switch manipulation. The switch was set to between 0 and 300 mW. By conducting several cycles of pump switch with a duration of 10 seconds, the RD-μFBG could completely be recycled with steep rising and falling edges, further underpinning the fast response regarding the pump switch. According to Fig. 5(d), the result of the cycling test in the air was not so smooth. The reason is attributed to the perturbation of the cross-ventilation mediated the light-induced heat. The air force exerted on the thinned fiber tip is reversible by the pump on and off, allowing future attempts on the light-induced shape modification to the fiber. By contrast, the RD-μFBG showed better performance in the cycling tests using pure ethanol and DI water due to the suppression of the light-induced force excreted by the liquid. The temperature steps of RD-μFBG reached 6 °C in pure ethanol and 4 °C in the water, as shown in Fig. 5(e) and (f), respectively, allowing instant self-photoheating and cooling of the device for the commonly used solvents.

6. Conclusion

In summary, the self-photoheating integrated microfiber Bragg grating refractive index sensor was proposed and experimentally demonstrated. The sensor was developed by etching an Er/Yb co-doped active fiber Bragg grating using the hydrofluoric acid. The approach can endow the grating with the ambient environment sensing ability without compromising the completeness of core structure for holding the active and photosensitive dopants. The μFBG presented a low RI detection limit of 4×10^{-4} RIU. As the pump laser was guided to the μFBG, the rare-earth dopants were excited to the higher energy level lying in the stimulated absorption and then mediated the heat releasing via non-radiative downward transition. Under 500 mW pumping, the μFBG could be warmed by an amount of 30 °C in the air, 8 °C in the ethanol, and 4 °C in the water (the latter two are the most commonly used solvents). The dynamic pumping results and pump switch tests elucidated that the self-heated sensor could answer the pump and off operation instantaneously. Future attempts based on this work should focus on the further improvement of temperature elevation ability and RI sensitivity of the sensor. For example, a higher absorption fiber and a higher resolution interrogation technique can be involved to address those problems, respectively. The multimode active fiber, which can resist the loss of the dopants after tapering, is envisioned to enhance the efficiency of device fabrication through the flame-tapering fiber thinning technique. A well-designed package structure, such as centrifuge tube fixation, can also contribute to the protection of the sensor head for future application. It is anticipated that the proof-of-concept of μFBG refractive index sensor incorporating the dynamic self-heat governing capability can dedicate itself to the biological, chemical, and environmental sensing areas.

References

[1] F. Chiavaioli, A. J. C. Gouveia, A. S. P. Jorge, and F. Baldini, "Towards a Uniform Metrological Assessment of Grating-Based Optical Fiber Sensors: From Refractometers to Biosensors," *Biosensors*, vol. 7, pp. 1–29, 2017.

[2] Y. Xu *et al.*, "Optical refractive index sensors with plasmonic and photonic structures: Promising and inconvenient truth," *Adv. Opt. Mater.,* vol. 7, 2019, Art. no. 1801433.

[3] Y. Zhao, X.-G. Hu, S. Hu, and Y. Peng, "Applications of fiber-optic biochemical sensor in microfluidic chips: A review," *Biosensors Bioelectron.,* vol. 166, 2020, Art. no. 112447.

[4] B.-O. Guan, and Y. Huang, "Interface sensitized optical microfiber biosensors," *J. Lightw. Technol.,* vol. 37, no. 11, pp. 2616–2622, Jun. 2019.

[5] R. Ismaeel, T. Lee, M. Ding, M. Belal, and G. Brambilla, "Optical microfiber passive components," *Laser Photon. Rev.,* vol. 7, pp. 350–384, 2013.

[6] J. Lou, Y. Wang, and L. Tong, "Microfiber Optical Sensors: A Review," *Sensors*, vol. 14, pp. 5823–5844, 2014.

[7] J. Chen, D. Li, and F. Xu, "Optical microfiber sensors: Sensing mechanisms, and recent advances," *J. Lightw. Technol.,* vol. 37, no. 11, pp. 2577–2589, Jun. 2019.

[8] L. Zhang, Y. Tang, and L. Tong, "Micro-/nanofiber optics: Merging photonics and material science on nanoscale for advanced sensing technology," *iScience,* vol. 23, 2020, Art. no. 100810.

[9] J.-L. Kou, M. Ding, J. Feng, Y.-Q. Lu, F. Xu, and G. Brambilla, "Microfiber-Based Bragg Gratings for Sensing Applications: A Review," *Sensors*, vol. 12, pp. 8861-8876, 2012.

[10] B.-O. Guan, J. Li, L. Jin, and Y. Ran, "Fiber Bragg gratings in optical microfibers," *Opt. Fiber Technol.,* vol. 19, pp. 793–801, 2013.

[11] Y. Wu *et al.*, "Graphene-coated microfiber Bragg grating for high-sensitivity gas sensing," *Opt. Lett.,* vol. 39, pp. 1235–1237, 2014.

[12] Y. Ran, P. Xiao, Y. Zhang, D. Hu, Z. Xu, L. Liang *et al.*, "A Miniature pH Probe Using Functional Microfiber Bragg Grating," *Optics*, vol. 1, pp. 202–212, 2020.

[13] A. N. Chryssis, S. S. Saini, S. M. Lee, Y. Hyunmin, W. E. Bentley, and M. Dagenais, "Detecting hybridization of DNA by highly sensitive evanescent field etched core fiber Bragg grating sensors," *IEEE J. Sel. Topics Quantum Electron.,* vol. 11, no. 4, pp. 864–872, Jul./Aug. 2005.

[14] D. Sun, T. Guo, Y. Ran, Y. Huang, and B.-O. Guan, "In-situ DNA hybridization detection with a reflective microfiber grating biosensor," *Biosensors Bioelectron.,* vol. 61, pp. 541–546, 2014.

[15] Y. Cao *et al.*, "Resolution-improved in situ DNA hybridization detection based on microwave photonic interrogation," *Opt. Exp.,* vol. 23, pp. 27061–27070, 2015.

[16] Y. Cao *et al.*, "High-resolution and temperature-compensational HER2 antigen detection based on microwave photonic interrogation," *Sensors Actuators B: Chem.,* vol. 245, pp. 583–589, 2017.

[17] T. Liu *et al.*, "A label-free cardiac biomarker immunosensor based on phase-shifted microfiber Bragg grating," *Biosensors Bioelectron.*, vol. 100, pp. 155–160, 2018.

[18] Y. Ran *et al.*, "Harmonic optical microfiber Bragg grating immunosensor for the accelerative test of cardiac biomarker (cTn-I)," *Biosensors Bioelectron.*, vol. 179, 2021, Art. no. 113081.

[19] S. Sridevi, K. S. Vasu, S. Asokan, and A. K. Sood, "Sensitive detection of C-reactive protein using optical fiber Bragg gratings," *Biosensors Bioelectron.*, vol. 65, pp. 251–256, 2015.
[20] A. Juste-Dolz *et al.*, "BIO Bragg gratings on microfibers for label-free biosensing," *Biosensors Bioelectron.*, vol. 176, 2021, Art. no. 112916.
[21] X. T. Gan *et al.*, "Graphene-assisted all-fiber phase shifter and switching," *Optica*, vol. 2, pp. 468–471, 2015.
[22] X. Gan *et al.*, "Graphene-controlled fiber Bragg grating and enabled optical bistability," *Opt. Lett.*, vol. 41, pp. 603–606, 2016.
[23] H. Li *et al.*, "Single-molecule detection of biomarker and localized cellular photothermal therapy using an optical microfiber with nanointerface," *Sci. Adv.*, vol. 5, 2019, Art. no. eaax4659.
[24] Y. Huang, P. Chen, H. Liang, A. Xiao, S. Zeng, and B.-O. Guan, "Nucleic acid hybridization on a plasmonic nanointerface of optical microfiber enables ultrahigh-sensitive detection and potential photothermal therapy," *Biosensors Bioelectron.*, vol. 156, 2020, Art. no. 112147.
[25] J. Koppert *et al.*, "Self-heating tilted fiber Bragg grating device for melt curve analysis of solid-phase DNA hybridization and thermal cycling," *Anal. Bioanalytical Chem.,* vol. 411, pp. 6813–6823, 2019.
[26] S. A. Alqarni, W. G. Willmore, J. Albert, and C. W. Smelser, "Self-monitored and optically powered fiber-optic device for localized hyperthermia and controlled cell death in vitro," *Appl. Opt.,* vol. 60, pp. 2400–2411, 2021.
[27] X. Yang *et al.*, "Microfiber interferometer integrated with au nanorods for an all-fiber phase shifter and switch," *Opt. Lett.*, vol. 44, pp. 1092–1095, 2019.
[28] L. Qi, L. Jin, Y. Liang, L. Cheng, and B. Guan, "Efficiency enhancement of optical tuning for Bragg gratings in rare-earth doped fibers," *IEEE Photon. Technol. Lett.*, vol. 26, no. 12, pp. 1188–1191, Jun. 2014.
[29] Y. Ran *et al.*, "193nm excimer laser inscribed Bragg gratings in microfibers for refractive index sensing," *Opt. Exp.*, vol. 19, pp. 18577–18583, 2011.
[30] Y. Ran, L. Jin, Y. Tan, L. Sun, J. Li, and B.-O. Guan, "High-efficiency ultraviolet inscription of Bragg gratings in microfibers," *IEEE Photon. J.*, vol. 4, no. 1, pp. 181–186, Feb. 2012.
[31] A. Iadicicco, A. Cusano, S. Campopiano, A. Cutolo, and M. Giordano, "Thinned fiber Bragg gratings as refractive index sensors," *IEEE Sensors J.*, vol. 5, no. 6, pp. 1288–1295, Dec. 2005.
[32] Y. Zha, Z. Xu, P. Xiao, F. Feng, Y. Ran, and B.-O. Guan, "Phase-shifted type-IIa fiber Bragg gratings for high-temperature laser applications," *Opt. Exp.*, vol. 27, pp. 4346–4353, 2019.
[33] H. K. Bal, Z. Brodzeli, N. M. Dragomir, S. F. Collins, and F. Sidiroglou, "Uniformly thinned optical fibers produced via HF etching with spectral and microscopic verification," *Appl. Opt.*, vol. 51, pp. 2282–2287, 2012.